Topics in Catalysis
https://doi.org/10.1007/s11244-023-01836-1

ORIGINAL PAPER

Bifunctional Pt Catalysts Supported on a Zeolite-Binder Matrix for the Hydrodeoxygenation of Isoeugenol for Renewable Jet Fuel Production

Mark E. Martínez-Klimov[1] · Päivi Mäki-Arvela[1] · Zuzana Vajglová[1] · Christoph Schmidt[1] · Olha Yevdokimova[1] · Markus Peurla[2] · Narendra Kumar[1] · Kari Eränen[1] · Dmitry Yu. Murzin[1]

Accepted: 6 June 2023

Abstract
Hydrodeoxygenation (HDO) of isoeugenol was carried out at 200 °C and 30 bar of H_2 in a batch reactor using a series of bifunctional catalysts consisting of platinum supported on zeolite H-Beta-25 or H-Beta-300 and Bindzil as a binder. The purpose of the matrix was to understand the effect of the binder on the reaction, emulating the components of industrial catalysts and therefore facilitating catalyst scale-up. The effect of the supports acid strength, the location of metal nanoparticles, and their proximity to acid sites was also studied. The catalysts were characterized by N_2 physisorption, inductively coupled plasma atomic emission spectrometry, Fourier transform infrared spectroscopy of adsorbed pyridine and scanning and transmission electron microscopy. It was found that platinum supported only on the zeolite was more active compared to platinum located on the binder. High levels of isoeugenol conversion (ca. 100%), propylcyclohexane yield (56%) and the liquid-phase mass balance (68%) were obtained for the catalyst consisting of Pt supported on both zeolite H-Beta-25 and Bindzil.

Keywords Hydrodeoxygenation · Bifunctional catalyst · Platinum · Zeolite · Bindzil · Binder · Isoeugenol

1 Introduction

An interest in developing alternative and renewable fuels has increased recently in a quest to reduce contaminant emissions and dependence on fossil fuels, as well as to meet climate regulations [1]. Currently, one of the main challenges for the energy transition of the aviation industry is that the fuels used in commercial planes cannot be replaced by batteries, mainly due to their low energy to weight ratio [2]. A viable alternative would be to obtain hydrocarbons from renewable sources, thus lowering their environmental impact [3, 4].

✉ Mark E. Martínez-Klimov
mklimov@abo.fi

✉ Dmitry Yu. Murzin
dmurzin@abo.fi

[1] Johan Gadolin Process Chemistry Centre, Åbo Akademi University, Henriksgatan 2, 20500 Turku/Åbo, Finland

[2] Institute of Biomedicine, University of Turku, Kiinamyllynkatu 10, 20520 Turku/Åbo, Finland

Among many renewable energy sources, lignocellulosic biomass is considered as an attractive source for biofuels, materials, and chemicals, due to its abundance and availability. Consisting of cellulose, hemicellulose, and lignin, it can be converted through thermochemical or chemical processes into highly desired compounds. While cellulose, hemicellulose and extractives are employed extensively within the pulp and papermaking industry and to produce fine chemicals [5, 6] respectively, lignin is yet to make a commercial breakthrough.

Recent research has focused on the valorization of lignin, a complex biopolymer rich in aromatics and oxygenated moieties. Pyrolysis of lignin results in a mixture of smaller oxygenated compounds commonly called lignin-derived bio-oil, which displays low heating value, high viscosity and corrosiveness caused by its oxygen content, thereby limiting its use as a fuel [7].

These oxygen moieties need to be removed to obtain hydrocarbons that can be utilized in modern combustion engines, which can be done through hydrodeoxygenation (HDO). Two types of active sites are required to carry out HDO: metal (to activate hydrogen) and acid sites or oxygen

Published online: 21 June 2023

vacancies (to activate the oxygen moieties in biomass-derived compounds) [8].

HDO of model phenolic compounds is commonly studied instead of bio-oil per se due to the complexity of the latter. Among the most commonly used molecules are phenol [9], guaiacol [10, 11] anisole [27] and vanillin [12]. Isoeugenol is of particular interest as it resembles the phenylpropane units constituting lignin and the molecules obtained from its pyrolysis; its HDO product being propylcyclohexane [13], which is within the hydrocarbon range utilized in jet fuel.

Renewable jet fuel must exhibit similar properties as conventional jet fuel in order to be used within existing infrastructure. In general, fossil-derived jet fuel consists of hydrocarbons in the range of C_8–C_{16}, with alkanes, alkenes, cycloalkanes, and aromatics being the main components [14, 15].

Recent development of HDO catalysts has shifted towards transition metals such as: Ni, Mo and Co [16, 17]. However, also noble metals such as Pt, Ru and Pd, deposited on a variety of supports including zeolites, metal oxides [18–20], different types of carbon [21–25], and nanostructured materials [26–28], have been investigated.

Zeolites are structured aluminosilicates of considerable interest, as they are one of the most extensively used supports and catalysts, mainly due to their inherent acidity (essential for HDO), large surface area and porosity [29]. Often used in petroleum refining and petrochemical industry (e.g., isomerization, alkylation, and cracking reactions [30]), they can be found either as naturally occurring minerals or synthesized ones, allowing to tune their acidity by varying their Si:Al ratio [31] depending on the desired use or target reaction. Research on the scaling-up of zeolite-based catalysts has recently become an attractive topic not only in industry, but also in academia [34, 36]. Catalysts used in industry need to be shaped to reduce pressure drops and resist the conditions used in continuous systems [32], which requires fundamental understanding of shaping processes such as extrusion, for example. Commercial catalyst extrudates are composed of a mixture of materials (a matrix), containing not only a metal and a support, but also a binder (10–35 wt%), as well as a number of other components [33]. Binders, usually alumino-silicate clays, are added to aid with the catalysts shaping and to provide mechanical strength. However, their effect on catalytic activity or other physical properties has been scarcely studied in academic research.

The importance of active site proximity for bifunctional catalysts containing a binder has been studied in several works in the literature, namely for hydroconversion reactions. It was found that close proximity between Pt and Beta zeolite resulted in higher conversion and C_6 selectivity for the hydroisomerization of n-hexane when using Pt supported on H-Beta-25 and Bentonite extrudates [34]. In contrast, close proximity between Pt and acid sites was detrimental for selectivity in the hydroisomerization of n-heptane when using catalysts comprised of zeolite ZSM-22 and mordenite and γ-alumina binder, as it resulted in undesired cracking reactions [35]. These results highlight the necessity of studying the effects of the intimacy between the sites for particular systems.

Our previous studies on the HDO of lignin-derived model compounds have focused on metal-support systems without considering the addition of a binder [44]. In a recent work [44], bifunctional Pt- and Ir-modified Beta zeolites and mesoporous materials (SiO_2, Al_2O_3 and MCM-41) were tested for the deoxygenation of isoeugenol in a batch reactor at 200 °C, 30 bar of total pressure and 4 h of the reaction time. While studying the effect of the support on the reaction, it was found that complete conversion of isoeugenol and up to 89% selectivity was achieved using Pt/H-Beta-300 in 240 min. The other supports tested displayed conversions of $< 10\%$, highlighting the importance of support acidity. An additional benefit of the zeolite-supported catalysts over other supports, such as activated carbon, is that it can be regenerated through calcination, while retaining similar catalytic activity.

In the present work, hydrodeoxygenation of isoeugenol over a bifunctional matrix consisting of Pt supported on zeolite Beta and Bindzil as a binder was studied. The former (zeolite Beta) was chosen due to its commercial availability and relatively big pore size, while the latter (Bindzil), a type of colloidal silica without impurities, allows easy shaping of the zeolite-based catalysts [36].

Several catalyst parameters were modified to better understand their effect on the reaction. First, a binder (Bindzil) was used in the matrix to observe its effect on the reaction. Two types of zeolites (H-Beta-25 and H-Beta-300) were used to determine the effect of acidity. Similarly, the location of Pt was also varied to determine the importance of the proximity between the active sites. Pt was alternatively loaded on Bindzil or on zeolite or on both. The results show that Pt location and the selection of catalyst preparation method have a large impact on the catalyst performance.

2 Experimental

2.1 Reagents

Zeolites NH_4-Beta-25 and H-Beta-300 were obtained from Zeolyst International ($SiO_2/Al_2O_3 = 25$ and $SiO_2/Al_2O_3 = 300$, respectively) while Binder Bindzil-50/80 (50% colloidal SiO_2 in H_2O) was obtained from AzkoNobel. Zeolite NH_4-Beta-25 was transformed into the proton form by calcination at 400 °C [37]. The platinum precursor, $[Pt(NH_3)_4](NO_3)_2$, ($\geq 50.0\%$ Pt basis) was acquired from Sigma-Aldrich. For the reactions, n-dodecane (Acros

Organics, 99%) and isoeugenol (Sigma Aldrich, 98%, mixture of cis and trans) were used.

2.2 Catalyst Synthesis

The location of the metal deposition was varied for both series of catalysts in order to modify the proximity between the metal and acid sites. Platinum was deposited by the evaporation-impregnation method. The nominal metal loading for all catalysts was 2 wt%. All catalysts have the same ratio of the zeolite-to-Bindzil of 70:30. The catalysts were denoted as either PtB300Z*X* or PtB25Z*X*, depending on the zeolite used as a support. Z was used to denote the presence of Bindzil while *X* corresponds to the location of the metal; A was used for Pt supported on both zeolite and the binder, B for Pt supported only on the zeolite, and C for Pt supported only on the binder. The preparation method has been thoroughly described in previous publications [37, 38]. The following is a brief summary:

Type A—Pt located on both: A mixture of 70% zeolite and 30% Bindzil in water (80% water to 20% mixture) was stirred for 24 h, followed by evaporation of water and calcination at 500 °C. After deposition of platinum from $[Pt(NH_3)_4](NO_3)_2$, the catalyst was reduced under hydrogen flow (40 mL/min) at 350 °C for 3 h with a heating rate of 2 °C/min.

Type B—Pt located on zeolite: First, platinum was deposited on the zeolite by evaporation-impregnation from $[Pt(NH_3)_4](NO_3)_2$ followed by reduction under hydrogen flow (40 mL/min) at 350 °C for 3 h with a heating ramp of 2 °C/min. Pt/zeolite was mixed afterwards with Bindzil in water for 24 h. After water was evaporated, the catalyst was calcined at 500 °C.

Type C—Pt located on binder: Bindzil was dried and sieved to a size of 45–63 µm prior to deposition of Pt. After deposition of platinum, Pt/Bindzil was reduced under hydrogen flow (40 mL/min) at 350 °C for 3 h with a heating ramp of 2 °C/min. Thereafter, it was mixed in water with the corresponding amount of the zeolite, followed by calcination of the catalyst at 500 °C.

All catalysts were sieved to a particle size of 45–63 µm to avoid internal mass transfer limitations.

A summary of the catalysts used in the current work is presented in Table 1.

2.3 Catalytic Tests

The catalysts were reduced *ex-situ* under continuous hydrogen flow (40 mL/min, 350 °C for 180 min, 10 °C/min) in a glass reactor. The system was flushed with argon (50 mL/min, 10 min) prior and after the reduction procedure to remove air and hydrogen, respectively. Dodecane, the solvent used in the reaction, was added to avoid reoxidation of the catalyst.

HDO reactions were performed in a stainless-steel batch reactor (PARR, 300 mL) equipped with a heating jacket and mechanical stirring, as well as a sampling, gas inlet and outlet valves. The following quantities were used for the reaction: 0.1 g of isoeugenol, 0.05 g of the catalyst, and 50 mL of dodecane.

After the reactant, the catalyst and the solvent were loaded into the reactor, it was purged with 7 bar of argon first (AGA, 99.999%) for 10 min and afterwards with 10 bar of hydrogen (AGA, 99.999%) for 10 min. The reactor was pressurized to an initial pressure of 20 bar with hydrogen. The reactor was heated to 200 °C with a heating ramp of 10 °C/min without stirring. When the reaction temperature was reached, hydrogen was added to reach 30 bar of total pressure and stirring was started with a speed of 900 rpm to avoid external mass transfer limitations. Reaction conditions we chosen based on our previous work [44].

The time zero was set when the reaction temperature and stirring speed were reached. Samples taken at regular time intervals were analyzed by GC (Agilent Technologies 6890N, 7683 Series Injector) and GC/MS (Agilent Technologies 6890, 7683 Series Injector) both equipped with a DB-1 capillary column (Agilent 122-103e, 30 m length, 250 µm internal diameter and 0.5 µm film thickness) using the following temperature program: 60 °C (5 min), 3 °C/min to 135 °C, and 15 °C/min to 300 °C. Helium was employed as a carrier gas (flow rate of 1.7 mL/min).

Table 1 Denomination and characteristics of the catalysts used for HDO of isoeugenol

Catalyst denomination	Metal deposition location	Zeolite	Binder	Metal	Nominal Pt loading (wt%)
PtB25Z**A**	On both	**H-Beta 25**	**Bindzil**	Platinum	2
PtB25Z**B**	On zeolite	**H-Beta 25**	Bindzil	Platinum	2
PtB25Z**C**	On binder	H-Beta 25	**Bindzil**	Platinum	2
PtB300Z**A**	On both	**H-Beta 300**	**Bindzil**	Platinum	2
PtB300Z**B**	On zeolite	**H-Beta 300**	Bindzil	Platinum	2
PtB300Z**C**	On binder	H-Beta 300	**Bindzil**	Platinum	2

Conversion of dihydroeugenol (X) was calculated using Eq. (1), where C_0 is the initial concentration of dihydroeugenol and C_{DH} is the concentration of dihydroeugenol at a given time:

$$X = \frac{C_0 - C_{DH}}{C_0} * 100 \quad (1)$$

The yield of propylcyclohexane (Y_{PCH}) was determined using the concentration of propylcyclohexane at a certain time (C_{PCH}) and the initial concentration of dihydroeugenol (C_0) as shown below:

$$Y_{PCH} = \frac{C_{PCH}}{C_0} * 100 \quad (2)$$

Selectivity towards propylcyclohexane (S_{PCH}) was calculated using Eq. (3), where C_{PCH} is the concentration of propylcyclohexane at a certain time and Σ_{prod} is the sum of concentrations of all products at the corresponding time:

$$S_{PCH} = \frac{C_{PCH}}{\Sigma_{prod.}} * 100 \quad (3)$$

Gas chromatography liquid phase analysis (GCLPA) was used to determine the mass balance of products remaining in the liquid phase:

$$GCLPA = \frac{\Sigma_{all}}{C_0} * 100 \quad (4)$$

In Eq. (4) Σ_{all} is the sum of the concentrations of reactants and products at a specific time while C_0 is the initial concentration of dihydroeugenol.

Rate constants were determined using numerical data fitting of the dihydroeugenol concentrations throughout all the reaction duration, employing Eq. (5) for a zero-order reaction implemented in Origin 2019 software:

$$C_{DH} - C_0 = -k_0 t \quad (5)$$

The zero-order reaction kinetics was used as it most adequately described the experimental data. In Eq. (5) C_{DH} is the concentration of dihydroeugenol at a given time, C_0 is the initial concentration of dihydroeugenol, k_0 is the zero-order rate constant and t is time.

2.4 Materials Characterization

Determination of the catalyst metal loadings was performed by inductively coupled plasma atomic emission spectrometry (ICP-AES, Goffin Meyvis Spectro Cirusccd).

Textural characteristics of the catalysts were determined by nitrogen physisorption (Micromeritics 3Flex-3500). For all catalysts containing zeolites, the Dubinin–Radushkevich method was used to determine the specific surface area while the density functional theory (NL-DFT) method was used to determine pore size distributions. For pure Bindzil the surface area and pore volumes were determined, respectively, using the BET and the BJH method for the desorption branch. The samples underwent a two-stage pretreatment. *Ex-situ* outgassing was done in a Micromeritics VacPrep 061 Sample Degas System under vacuum at 200 °C for 20–24 h, followed by in-situ degassing for 5 h at 250 °C.

Metal particle sizes of the reduced catalysts were measured by transmission electron microscopy (JEM-1400Plus, JEOL, Japan). The samples were suspended in ethanol and mounted on a copper grid prior to the analysis. Determination of the average metal particle size was performed by measuring the diameter of over 200 particles using the ImageJ software. On average 8–10 images per sample have been evaluated.

Scanning electron microscopy (Zeiss Leo Gemini 1530) was utilized to observe the morphological differences between the supports.

Quantification of the Brønsted and Lewis acid sites of the catalysts was done by Fourier transform infrared spectroscopy of adsorbed pyridine (ATI Mattson FTIR Infinity Series) using molar extinction coefficients reported in the literature [39]. Desorption of pyridine at 250, 350, and 450 °C was done to determine the weak, medium, and strong acid sites, respectively; measurements were taken at 100 °C.

3 Results and Discussion

3.1 Catalyst Characterization

Morphological differences among the zeolites, Bindzil and the mixture of the zeolite and Bindzil can be observed using scanning electron microscopy (Fig. 1). H-Beta-25 particles are much smaller (ca. 20–250 nm, Fig. 1a) than those from H-Beta-300 (ca. 300–1000 nm, Fig. 1b). On the other hand, Bindzil displays mostly spherical particles (ca. 50–200 nm, Fig. 1c). For zeolite and Bindzil mixtures (Fig. 1d,e), it can be observed that the zeolitic particles are surrounded by the spherical Bindzil particles.

A summary of the metal loadings, metal particle sizes and textural properties of the catalysts and pure supports is presented in Table 2.

The catalyst metal loadings obtained by ICP were close to the nominal value of 2 wt%.

Transmission electron microscopy images (Fig. 2) were used to determine the metal particle sizes; a summary is presented in Table 2. All catalysts exhibited an average metal particle size in the range of 4–5 nm, indicating that the metal dispersion was 20–25%. Particle size histograms can be consulted in the supporting information, Fig. S1. Dispersion was calculated based on [40] using the formula

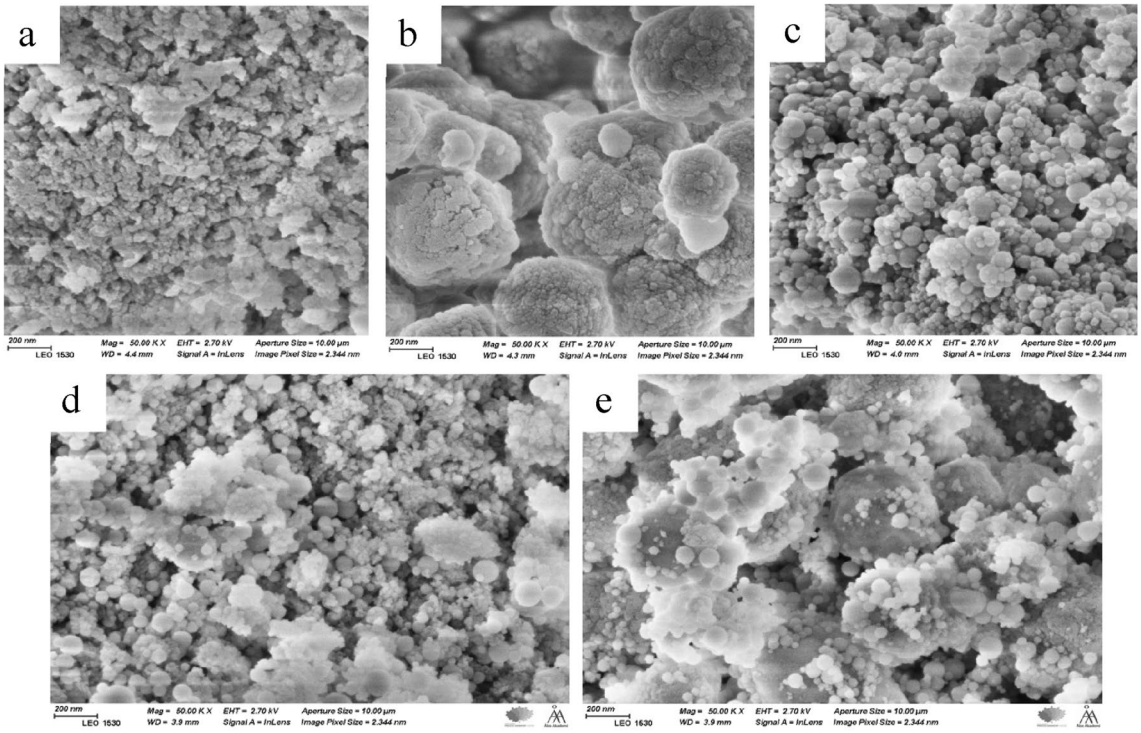

Fig. 1 SEM images of **a** H-Beta-25, **b** H-Beta-300, **c** Bindzil, **d** H-Beta-25 + Bindzil and **e** H-Beta-300 + Bindzil

Table 2 Metal loadings, metal particle sizes and textural properties of supports and catalysts

Catalyst	Pt loading (wt%)	Metal particle size (nm)	Textural characteristics		
			SSA (m^2/g)	V_Σ (cm^3/g)	V_{MP} (cm^3/g)
H-Beta-25	–	–	638	0.36	0.31
H-Beta-300	–	–	617	0.29	0.19
Bindzil	–	–	154	0.30	–
PtB25Z**A**	1.9	4.2	490	0.31	0.13
PtB25Z**B**	1.8	4.3	466	0.29	0.11
PtB25Z**C**	1.9	4.7	493	0.32	0.14
PtB300Z**A**	1.7	4.4	459	0.23	0.15
PtB300Z**B**	1.8	4.2	443	0.22	0.14
PtB300Z**C**	1.8	4.6	467	0.26	0.15
PtB300Z**A** (spent)	n.d	4.7	432	0.20	0.12
PtB300Z**B** (spent)	n.d	4.8	421	0.18	0.11
PtB300Z**C** (spent)	n.d	5.3	425	0.21	0.13

n.d. not determined

$d_{Pt} = 108/D(\%)$. Dispersion values were similar between samples given their similar metal particle sizes. The presence of bigger particles (up to 50 nm) was observed in the case of both PtB300ZC and PtB25ZC, where Pt was deposited on Bindzil. This could be caused by the preparation of these materials; namely deposition of platinum only on a lower amount of the support (29 wt% corresponding to Bindzil) and different point zero charges (pzc) of zeolites and Bindzil. The latter difference implies also differences between the zeta potential of these materials at the pH of deposition and pzc, resulting in different degree of Pt agglomeration on the zeolite and the binder.

TEM micrographs of spent PtB300Z*X* catalysts are shown in Fig. 3 and the corresponding average metal particle sizes are presented in Table 2. A slight increase in metal particle size was observed for spent catalysts, indicating that agglomeration occurred during the catalytic reactions.

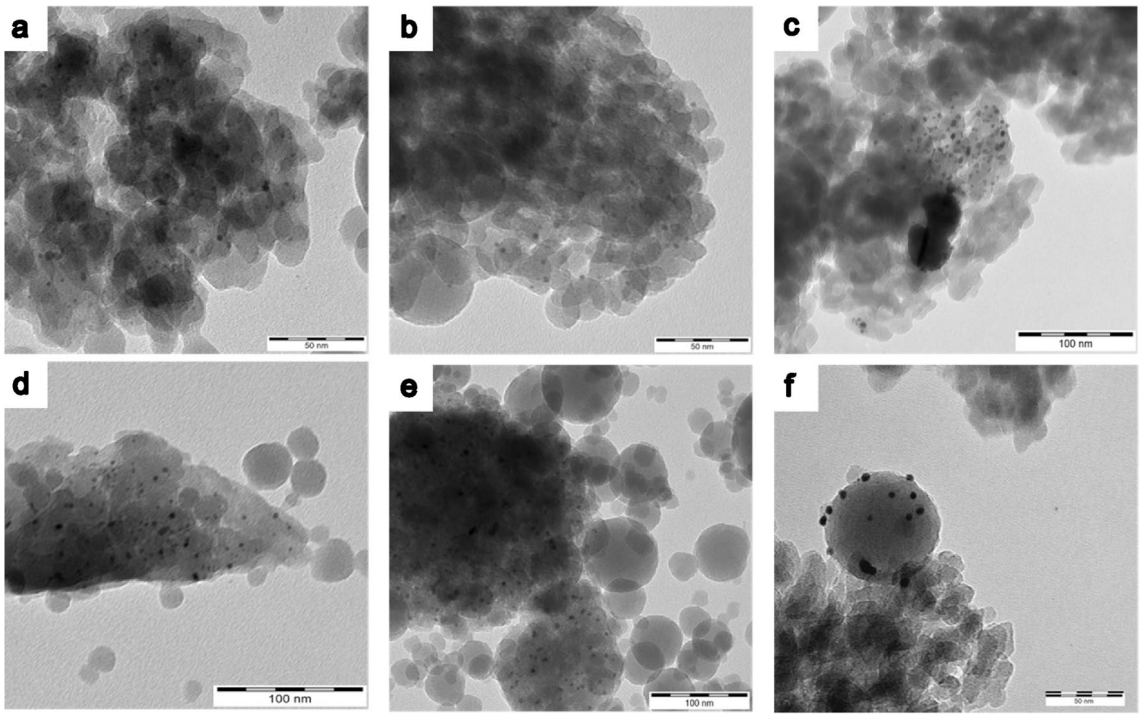

Fig. 2 TEM images of fresh **a** PtB25ZA, **b** PtB25ZB, **c** PtB25ZC and **d** PtB300ZA, **e** PtB300ZB, **f** PtB300ZC catalysts

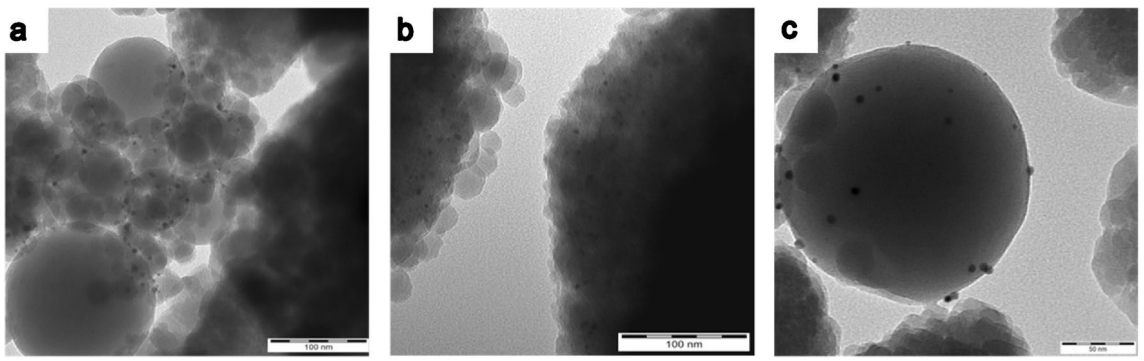

Fig. 3 TEM micrographs of spent **a** PtB300ZA, **b** PtB300ZB and **c** PtB300ZC

According to the nitrogen physisorption measurements, the catalysts exhibited high specific surface (SSA) areas (ca. 450 m^2/g), as well as total pore volume (V_Σ) of 0.2–0.3 cm^3/g and a pore diameter of 0.6 nm.

A decrease in the surface area and the micropore volume (V_{MP}) can be observed when comparing the catalysts to the corresponding pure zeolitic supports, which could be explained by the presence of Bindzil with a lower surface area (154 m^2/g), in addition to the blockage of the micropores during metal deposition. Among the catalysts, those supported on H-Beta-25 displayed higher SSA and higher total pore volume (V_Σ) than those supported on H-Beta-300. The pore diameter for all zeolitic-based catalysts was ca. 0.6 nm, indicating microporosity. On the other hand, neat Bindzil displayed a pore size of 12 nm due to its mesoporosity.

The textural properties of the spent H-Beta-300 catalysts were also measured after being washed with 100 mL of acetone. The same degassing procedure as for the fresh catalysts was followed. A slight decrease in the textural properties can be observed when comparing with the corresponding fresh catalysts; this could be caused by coke formation during the reaction.

Adsorption–desorption isotherms and the pore size distributions are presented in Fig. 4.

Figure 4a illustrates the difference in isotherm profiles between zeolites and the colloidal silica (Bindzil).

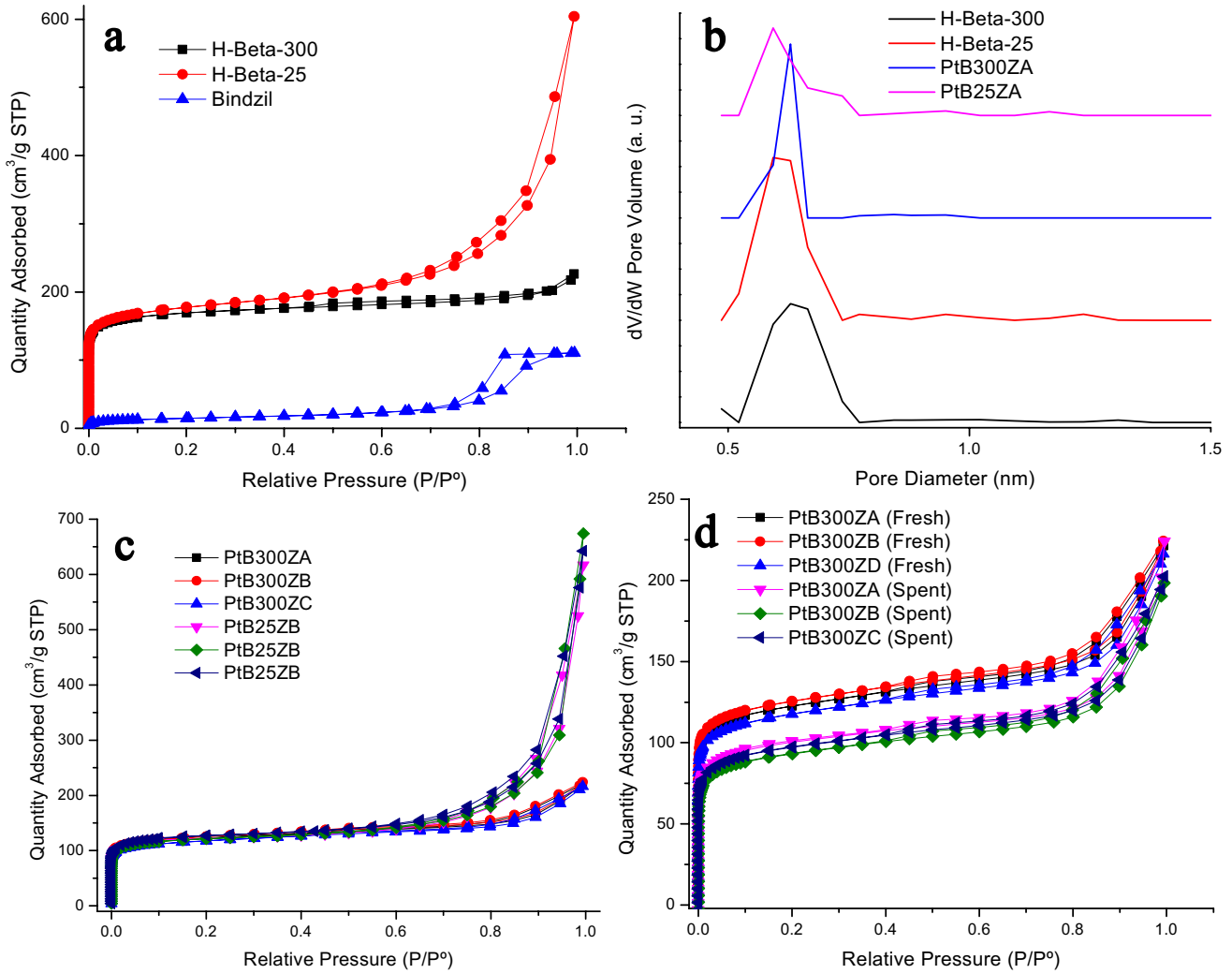

Fig. 4 **a** Adsorption–desorption isotherms of zeolites H-Beta-300, H-Beta-25 and Bindzil, **b** pore size distribution of zeolites H-Beta-25, H-Beta-300, and catalysts PtB300ZA and PtB25ZA, **c** adsorption–desorption isotherm comparison of both series of catalysts and **d** adsorption–desorption isotherm comparison of fresh and spent PtB300Z*X* catalysts

Both zeolites display type I isotherms, characteristic of microporous materials [41]. Zeolite H-Beta-25 exhibits an H3 hysteresis type, while Bindzil displays a type IV isotherm and hysteresis H2, due to mesoporosity. The main pore contribution obtained by NL-DFT (Fig. 4b) was ca. 0.6 nm for pure zeolites and all catalysts. The catalysts maintained similar adsorption–desorption isotherms to their corresponding zeolite support (Fig. 4c) and no changes in microporosity were observed after addition of the binder.

A noticeable difference in the adsorption isotherms could be observed in Fig. 4d between fresh and spent PtB300Z*X* catalysts, which also resulted in decreased textural properties of spent catalysts (Table 2). This could be due to the formation of carbon deposits during the reaction.

Pyridine FTIR was used to measure the acid site amount and strength of the catalysts and pure supports, results are presented in Table 3.

As expected, pure H-Beta-25 displayed the highest acidity, over 4 times higher than H-Beta-300. On the other hand, Bindzil contained the lowest amount of acid sites. Addition of Bindzil to the catalyst mixture resulted in a decrease in overall acidity, as expected, being also in line with changes in the textural properties obtained from nitrogen physisorption. The catalysts containing H-Beta-25 were more acidic than those with H-Beta-300. A trend was observed for both series of catalysts. The most acidic catalyst was type C, where Pt was located on the binder, indicating that deposition of the metal affected zeolite acidity, as previously reported in the literature [42]. The catalyst with the highest amount of acid sites was PtB25Z**C**. All catalysts from

Table 3 Support and catalyst acidity determined by Pyridine FTIR

Catalyst	Brønsted acid sites (μmol/g)*			Lewis acid sites (μmol/g)*			Total acid sites (μmol/g)		
	W	M	S	W	M	S	BAS	LAS	Total
H-Beta-25	67	33	129	26	5	6	229	37	266
H-Beta-300	7	29	19	4	1	1	55	6	61
Bindzil	12	0	0	3	0	0	12	3	15
PtB25Z**A**	44	10	4	12	4	2	58	18	76
PtB25Z**B**	51	4	8	7	2	4	63	13	76
PtB25Z**C**	61	4	28	8	1	11	93	20	113
PtB300Z**A**	9	2	0	5	3	0	11	8	19
PtB300Z**B**	6	2	0	6	0	0	8	6	14
PtB300Z**C**	10	8	0	13	2	0	18	15	33

*Desorption of pyridine at 250, 350, and 450 °C was done to determine the weak, medium, and strong acid sites, respectively; measurements were taken at 100 °C

the PtB300Z*X* series based on beta-300 with a high ratio of silica to alumina lacked strong acid sites.

3.2 Hydrodeoxygenation of Isoeugenol

Hydrodeoxygenation (HDO) of isoeugenol (IE) was performed in a batch reactor at 200 °C.

The transformation of isoeugenol into dihydroeugenol (DH) occurred almost instantaneously, reaching 100% conversion within 1 min of reaction time. Subsequently, conversion of dihydroeugenol was followed [43]. The steps comprising the reaction network (Scheme 1) that follow are hydrogenation of the aromatic ring, dehydration, and demethoxylation, resulting in formation of the propylcyclohexane (PCH) desired product. A comparison of the catalytic results for HDO of isoeugenol using Pt/zeolite without the binder and both series of catalysts with the binder, under the same conditions, is presented in Table 4. The corresponding graphs for the catalytic activity; dihydroeugenol (DH) conversion, propylcyclohexane (PCH) yield and gas chromatography liquid phase analysis (GCLPA) for both series of catalysts are displayed in Fig. 5.

Catalysts Pt/H-Beta-25 and Pt/H-Beta-300 without a binder (Pt/B25 and Pt/B300, respectively) were included in entries 1 and 2 as a comparison. These values were obtained from a previous publication [44]. Entries 3–5 correspond to the catalysts containing zeolite H-Beta-25, while entries 6–8 correspond to those containing H-Beta-300.

Overall, activity was higher for catalysts without a binder (entries 1 and 2). For the binder-containing catalysts, the rate constant (k) values were the highest for catalysts PtB25ZB and PtB300ZA in their corresponding series ($3.8{\cdot}10^{-2}$ and $1.6{\cdot}10^{-2}$ M h^{-1} $g_{cat}{}^{-1}$, entries 4 and 6, respectively). Although these values are in the same order of magnitude as those obtained for Pt/B25 and Pt/B300 [44], they are 2–4 times lower, indicating that when using catalysts containing a binder, activity is lower than when using only Pt on zeolite. Such differences in catalytic activity could be attributed to addition of the binder, which resulted in considerable changes in acidity and the surface area. This is especially noticeable when comparing acidity of Pt/B300 (TAS = 52 μmol/g, [44]) and Pt/B25 (TAS = 406 μmol/g, [44]) and the series of catalysts containing Bindzil. Acidity for Pt/B300 is more similar to acidity of PtB25ZX series (TAS = 76–113 μmol/g) than of PtB300ZX series in the current work. Additionally, the zeolite fraction for the binder-containing catalysts is lower due to the addition of Bindzil, which is not the case for Pt/B300 and Pt/B25 used in [44].

Activity of the different catalysts towards DH transformation varies very much, as can be seen in Fig. 5a and Table 4. Dihydroeugenol (DH) conversion was higher for catalysts without a binder (entries 1 and 2), reaching 100% for both at 4 h of the reaction time, thus highlighting the effect of Bindzil addition on the catalytic activity. For both series of catalysts containing Bindzil, it can be observed that DH conversion is higher for the PtB25Z*X* series (78–53%) than for PtB300Z*X* (61–25%). Deactivation could also be observed for PtB300ZC catalyst, as DH conversion did not increase considerably after the initial period, which was not the case for all other catalysts. While the results further indicate that acidity plays a crucial role, its impact is not straightforward.

The most active catalysts for both Bindzil-containing series were those of type A and B (DH conversion of about 80% for PtB25ZA and PtB25ZB, entries 3 and 4; and 61% for PtB300ZA, entry 6).

In contrast, catalysts of the type C displayed the lowest conversions, almost half of that of type B (DH conversion of 53% for PtB25ZC, entry 5; and 25% for PtB300ZC, entry 8). This indicates that proximity between the acid sites and the metal particles is beneficial for the reaction giving improved activity. In these catalysts, Pt is located on the non-acidic Bindzil; therefore, further from the acid sites of the zeolites.

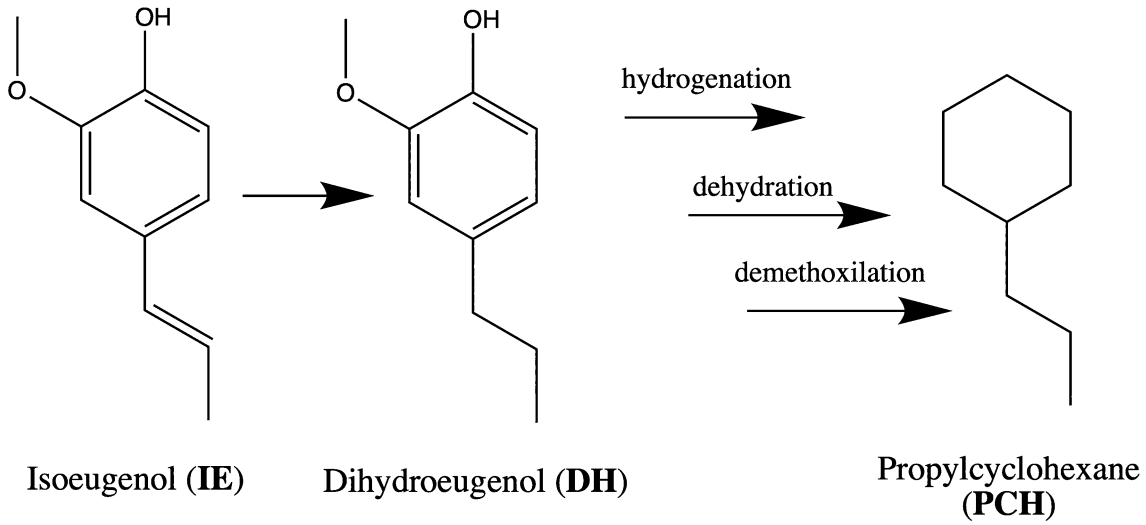

Scheme 1 A general reaction network for hydrodeoxygenation of isoeugenol

Additionally, the metal particle sizes for catalysts of type C were larger than for other types, contributing to a decrease in activity. The catalysts of type A displayed a slightly lower DH conversion than the catalysts of type B, which can be explained by a lower amount of Pt located on zeolites, as platinum was deposited on both the zeolite and the binder.

Gas Chromatography Liquid Phase Analysis (GCLPA) is a mass balance approximation for the reactants and products remaining in the liquid phase, as gaseous and heavy products (dimers, trimers, etc.…) have not been quantified. As presented in Table 4, GCLPA values decreased with the increase of DH conversion. This is generally due to the formation of products in the gas phase, such as water or methanol, which were not analyzed. The differences that are observed when comparing the GCLPA of catalysts with similar DH conversion, such as PtB25ZC (DH conversion = 53%, GCLPA = 66 entry 5) and PtB300ZA (DH conversion = 61%, GCLPA = 78%, entry 6) can be caused by formation of the oligomerization products, such as dimers, or by cracking/isomerization of the reactant, both of which were not measured, but have been reported in the literature [44].

The yield of propylcyclohexane (75%) and the reaction rate constant ($8.0 \cdot 10^{-2}$ M h^{-1} g_{cat}^{-1}) were the highest for Pt/

Table 4 Catalytic activity of PtB300Z*X* and PtB25Z*X* series of catalysts in hydrodeoxygenation of isoeugenol, performed in a batch reactor at 200 °C and 30 bar of H_2

Entry	Catalyst	IE conversion (%)[a]	DH conversion (%)[a]	k ·10^2 (M h^{-1} g_{cat}^{-1})[b]	GCLPA (%)[a,c]	PCH yield (%)[a]	PCH selectivity (%)[d]
1	Pt/B25[e]	100[e]	100[e]	6.4[e]	45[e]	55[e]	93[e]
2	Pt/B300[e]	100[e]	100[e]	8.0[e]	61[e]	75[e]	96[e]
3	PtB25Z**A**	100	78	3.7	68	56	82
4	PtB25Z**B**	100	82	3.8	62	53	81
5	PtB25Z**C**	100	53	2.8	66	21	79
6	PtB300Z**A**	100	61	1.6	78	45	84
7	PtB300Z**B**	100	46	1.5	85	37	92
8	PtB300Z**C**	100	25	0.8	83	6	n.d

n.d. not determined

[a]Values determined at 4 h of the reaction time

[b]Values for the rate constant (k) have been determined using a curve fitting method, considering the time dependent dihydroeugenol concentration

[c]Gas chromatography liquid phase analysis (GCLPA) is a mass balance approximation for the liquid phase

[d]Selectivity estimated at 40% DH conversion

[e]Values obtained from Ref. [44]

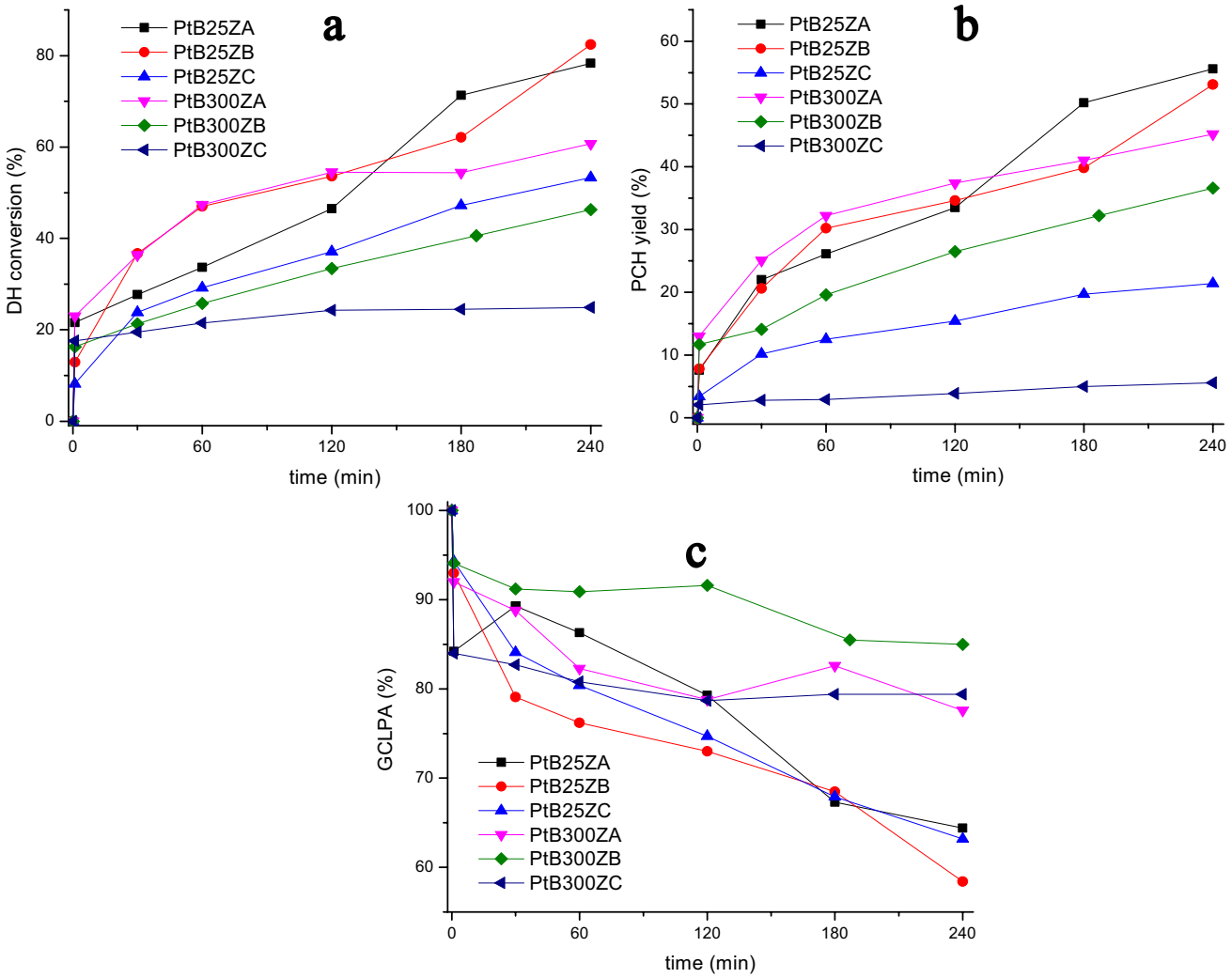

Fig. 5 Transformations of isoeugenol at 200 °C and 30 bar of H_2 **a** dihydroeugenol conversion, **b** propylcyclohexane yield and **c** GCLPA as a function of time

B300. It is important to note that in entries 1 and 2, the secondary products formed were 1-methyl-4-ethylcyclohexane and 1-methyl-2-propyl-cyclohexane, which are isomerization products. Zeolite H-Beta-25 has more total and strong acid sites than H-Beta-300, which could explain its lower selectivity to PCH due to secondary reactions.

On the other hand, the secondary product obtained when using the catalysts containing Bindzil was 2-methoxy-4-propylcyclohexanol, an oxygenated intermediate determined by GC–MS. This indicates that lower amounts of isomerization or cracking products for the Bindzil-containing catalysts could be due to their overall lower acidity. As observed from Pyridine FTIR results (Table 3), addition of the binder decreased the amount of total and strong acid sites. Such sites can lead to secondary reactions and deactivation of the catalyst, resulting in lower activity and selectivity [44].

While the catalysts containing more acidic zeolite H-Beta-25 display higher activity and yield of propylcyclohexane, the catalysts with H-Beta-300 zeolite exhibited higher selectivity (> 84%). Additionally, the PtB300ZA catalyst afforded a relatively high PCH yield (45%, entry 6), comparable to that of catalysts containing H-Beta-25. These results are in accordance with our previous publication when Pt/B25 displayed lower selectivity towards propylcyclohexane [44].

Interestingly, propylcyclohexane (PCH) yields were higher in both series for catalysts of type A (PCH yield of 56% for PtB25ZA, entry 3; and 45% for PtB300ZA, entry 6), which could also be caused by a higher dispersion of the

metal particles, i.e. their smaller cluster size, as in this type of catalyst, Pt was located on both zeolite and Bindzil.

Selectivity towards PCH was estimated for 40% DH conversion to be able to compare the values for different catalysts. As mentioned previously, higher PCH selectivities were obtained for PtB300ZA and PtB300ZB catalysts (> 84%, entries 6 and 7) which follows the same trend as observed for catalysts without Bindzil (entries 1–2). Furthermore, PCH selectivity for PtB300ZB (92%, entry 7) is comparable to that displayed by Pt/B25 and Pt/B300 (ca. 95%, entries 1–2). In the PtB300Z*X* series of catalysts, the lowest PCH selectivity was obtained for the catalyst of type A (PCH selectivity of 84%, entry 6).

From Fig. 5 it can be inferred that proximity between Pt particles (metal sites) and acid sites of the zeolites is important for hydrodeoxygenation. Additionally, the PtB25Z*X* series displayed higher DH conversion and PCH yield, indicating the effect of higher acidity on the catalytic activity. A clear difference in the GCLPA for both series of catalysts can also be observed in Fig. 5c, pointing out the formation of side products when using more acidic catalysts, as previously discussed. The effect of metal location and acidity on activity can be better observed in Fig. 6.

In Fig. 6a it can be observed that while dihydroeugenol conversion is higher for catalysts supported on H-Beta-25, the yield of propylcyclohexane for PtB300ZA catalyst is similar despite having almost four-fold fewer acid sites, which indicates that such high acidity is not necessary to obtain the same amount of the desired deoxygenation product. This conclusion is further illustrated in Fig. 6b,c. When comparing the rate constants to the total amount of acid sites (Fig. 6b) it can be observed that the PtB25Z*X* series (higher acidity) displays higher conversion. However, the PtB300Z*X* series displays similar yields of propylcyclohexane (Fig. 6c).

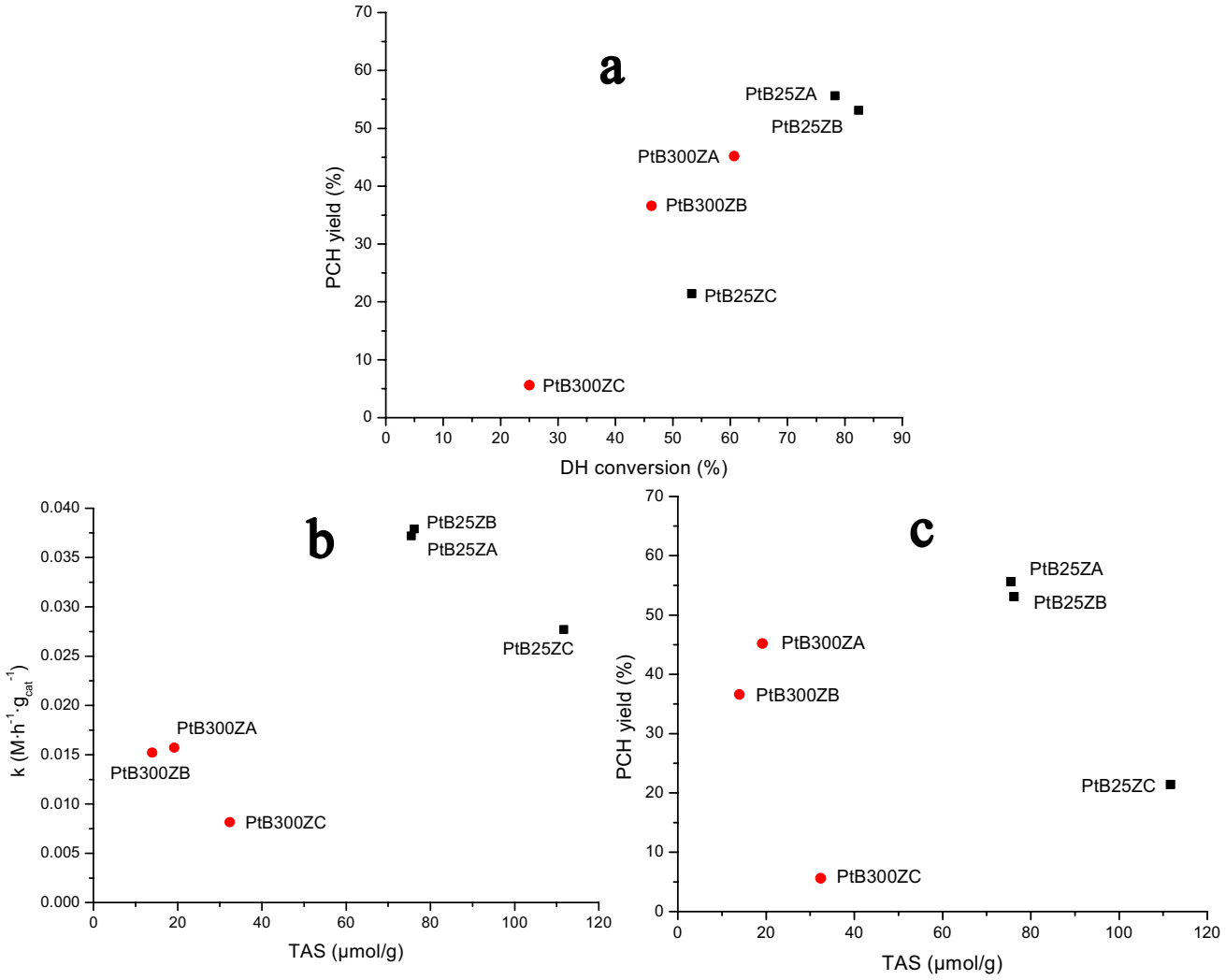

Fig. 6 Transformations of isoeugenol at 200 °C and 30 bar of H_2 **a** propylcyclohexane yield vs. dihydroeugenol conversion, **b** rate constant vs. total acid sites and **c** propylcyclohexane yield vs. total acid sites

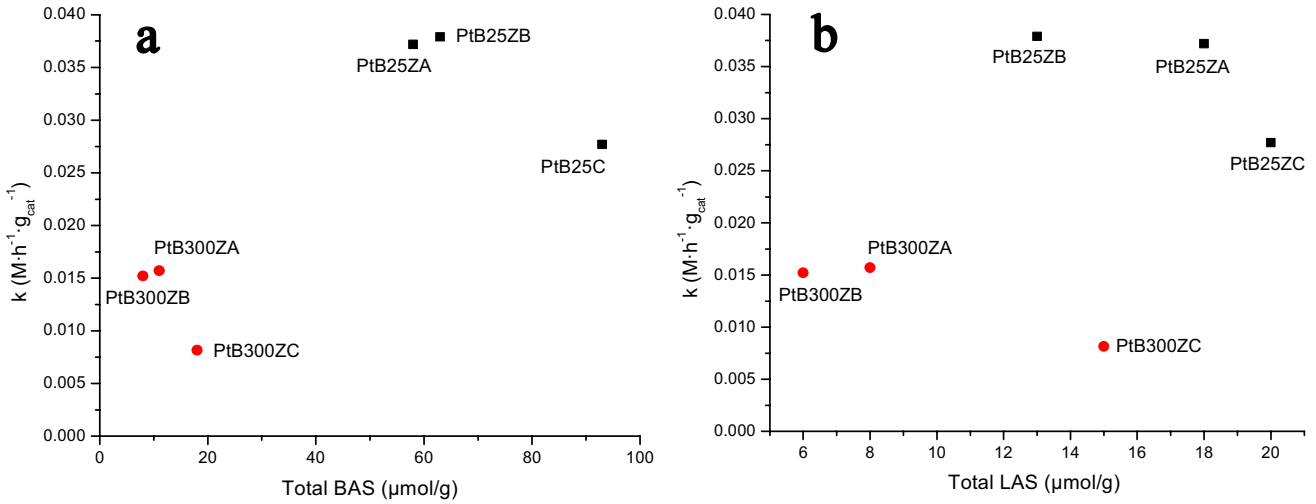

Fig. 7 Transformations of dihydroeugenol at 200 °C and 30 bar of H_2: **a** rate constants vs. total Brønsted acid sites and **b** rate constants vs. total Lewis acid sites

In Fig. 7 the relationship between the rate constants and the total amount of different acid sites (Brønsted and Lewis) is displayed.

Figure 7 seems to indicate that there is an optimum level of acidity for the hydrodeoxygenation of isoeugenol under the conditions and catalysts tested. In this case, the PtB25ZB catalyst displayed intermediate acidity among the tested catalysts and thus higher values for the rate constant.

Dispersion of Pt was similar for all catalysts (20–25%); therefore, we cannot attribute worse behavior of C catalysts to worse dispersion of Pt. In this case, acidity of the zeolites is necessary for HDO to activate the oxygen moieties on acid sites and carry out dehydration and demethoxylation reactions.

Our findings suggest that proximity between two types of active sites is necessary for catalytic performance. It has been documented in the literature [25] that acid sites or oxygen vacancies, provided by the support or oxophilic metals, are required to carry out the deoxygenation (hydrogenolysis of C-O bond) in HDO.

4 Conclusions

A catalytic matrix comprising 2 wt% of platinum supported on 69 wt% of zeolite H-Beta-300 or H-Beta25, and 29 wt% of Bindzil as a binder, displayed high activity for the hydrodeoxygenation of isoeugenol at 200 °C and 30 bar of hydrogen pressure. The effects of the binder addition, acidity of the zeolite and the metal location, were studied. Addition of Bindzil resulted in a decrease of the surface area and the total amount of acid sites when compared to the unmodified zeolite. The location of the platinum was varied depending on its deposition, whether it was on the zeolite, the binder or both. The deposition of platinum on the zeolite also resulted in a decrease in acidity. These changes reflected considerably the catalytic activity. Overall, the catalysts where Pt was located closer to the acid sites (being deposited on only zeolite or both zeolite and the binder) displayed higher dihydroeugenol conversion and propylcyclohexane yield, while deposition of platinum on the binder gave the lowest activity. Furthermore, while catalysts containing a more acidic zeolite (H-Beta-25) displayed higher activity, catalysts with Pt on the binder and H-Beta-300 displayed a similar propylcyclohexane yield. Results suggest that an optimum acidity is required for complete deoxygenation of isoeugenol. The highest selectivity to propylcyclohexane of 92% with 85% mass balance closure in the liquid phase was achieved for the catalyst when platinum was located only on the H-Beta zeolite with silica to alumina ratio of 300, while the highest conversion of dihydroeugenol of 82% and the yield of propylcyclohexane of 53% was obtained for the catalyst where platinum was located on both zeolite H-Beta with a silica to aluminum ratio 25 and the binder.

Supplementary Information The online version contains supplementary material available at https://doi.org/10.1007/s11244-023-01836-1.

Acknowledgements The authors would like to acknowledge the Electron Microscopy Laboratory, Institute of Biomedicine, University of Turku, and Biocenter Finland for access to Transmission Electron Microscopy. This work was supported by the Magnus Ehrnrooth Foundation.

Funding Open access funding provided by Abo Akademi University (ABO).

Data availability Data will be available upon request.

References

1. Markard J (2018) The next phase of the energy transition and its implications for research and policy. Nat Energy 3(8):628–633. https://doi.org/10.1038/s41560-018-0171-7
2. Kammermann J, Bolvashenkov I, Tran K, Herzog HG, Frenkel I (2020) Feasibility study for a full-electric aircraft considering weight, volume, and reliability requirements. In: International conference on electrotechnical complexes and systems (ICOECS) 1–6. https://doi.org/10.1109/ICOECS50468.2020.9278461
3. Wei H, Liu W, Chen X, Yang Q, Li J, Chen H (2019) Renewable bio-jet fuel production for aviation: a review. Fuel 254:115599. https://doi.org/10.1016/j.fuel.2019.06.007
4. Field CB, Campbell JE, Lobell DB (2008) Biomass energy: the scale of the potential resource. Trends Ecol Evol 23(2):65–72. https://doi.org/10.1016/j.tree.2007.12.001
5. Miura M, Shimotori Y, Nakatani H, Harada A, Aoyama M (2015) Bioconversion of birch wood hemicellulose hydrolyzate to xylitol. Appl Biochem Biotechnol 176(3):947–955. https://doi.org/10.1007/s12010-015-1604-4
6. Delbecq F, Wang Y, Muralidhara A, El Ouardi K, Marlair G, Len C (2018) Hydrolysis of hemicellulose and derivatives—a review of recent advances in the production of furfural. Front Chem. 6. https://doi.org/10.3389/fchem.2018.00146
7. Meng J, Moore A, Tilotta D, Kelley S, Park S (2014) Toward understanding of bio-oil aging: accelerated aging of bio-oil fractions. ACS Sustain Chem Eng 2(8):2011–2018. https://doi.org/10.1021/sc500223e
8. Wang X, Arai M, Wu Q, Zhang C, Zhao F (2020) Hydrodeoxygenation of lignin-derived phenolics—a review on the active sites of supported metal catalysts. Green Chem 22(23):8140–8168. https://doi.org/10.1039/D0GC02610G
9. Berenguer A, Sankaranarayanan TM, Gómez G, Moreno I, Coronado JM, Pizarro P, Serrano DP (2016) Evaluation of transition metal phosphides supported on ordered mesoporous materials as catalysts for phenol hydrodeoxygenation. Green Chem 18(7):1938–1951. https://doi.org/10.1039/C5GC02188J
10. Sulman A, Mäki-Arvela P, Bomont L, Alda-Onggar M, Fedorov V, Russo V, Eränen K, Peurla M, Akhmetzyanova U, Skuhrovcová L, Tišler Z, Grénman H, Wärnå J, Murzin DY (201) Kinetic and thermodynamic analysis of guaiacol hydrodeoxygenation. Catal Letter 149(9):2453–2467. https://doi.org/10.1007/s10562-019-02856-x
11. Gao D, Xiao Y, Varma A (2015) Guaiacol hydrodeoxygenation over platinum catalyst: reaction pathways and kinetics. Ind Eng Chem Res 54(43):10638–10644. https://doi.org/10.1021/acs.iecr.5b02940
12. Santos JL, Alda-Onggar M, Fedorov V, Peurla M, Eränen K, Mäki-Arvela P, Centeno MÁ, Murzin DY (2018) Hydrodeoxygenation of vanillin over carbon supported metal catalysts. Appl Catal A 561:137–149. https://doi.org/10.1016/j.apcata.2018.05.010
13. Lyu G, Wu S, Zhang H (2013) Estimation and comparison of bio-oil components from different pyrolysis conditions. Front Energy Res 3(28):1–11. https://doi.org/10.3389/fenrg.2015.00028
14. Hileman JI, Stratton RW (2014) Alternative jet fuel feasibility. Transp Policy 34:52–62. https://doi.org/10.1016/j.tranpol.2014.02.018
15. Kallio P, Pásztor A, Akhtar MK, Jones PR (2014) Renewable jet fuel. Curr Opin Biotechnol 26:50–55. https://doi.org/10.1016/j.copbio.2013.09.006
16. Mortensen PM, Grunwaldt JD, Jensen PA, Jensen AD (2016) Influence on nickel particle size on the hydrodeoxygenation of phenol over Ni/SiO2. Catal Today 259:277–284. https://doi.org/10.1016/j.cattod.2015.08.022
17. Bakhtyari A, Rahimpour MR, Raeissi S (2020) Cobalt-molybdenum catalysts for the hydrodeoxygenation of cyclohexanone. Renew Energy 150:443–455. https://doi.org/10.1016/j.renene.2019.12.119
18. Lu M, Du H, Wei B, Zhu J, Li M, Shan Y, Song C (2017) Catalytic hydrodeoxygenation of guaiacol over palladium catalyst on different titania supports. Energy Fuels 31(10):10858–10865. https://doi.org/10.1021/acs.energyfuels.7b01498
19. Mäkelä E, González Escobedo JL, Lindblad M, Käldström M, Meriö-Talvio H, Jiang H, Puurunen RL, Karinen R (2020) Hydrodeoxygenation of levulinic acid dimers on a zirconia-supported ruthenium catalyst. Catalysts 10(2):200. https://doi.org/10.3390/catal10020200
20. Afrin S, Bollini P (2019) Cerium oxide catalyzes the selective vapor phase hydrodeoxygenation of anisole to benzene at ambient pressures of hydrogen. Ind Eng Chem Res 58:14603–14607. https://doi.org/10.1021/acs.iecr.9b01987
21. Ohta H, Kobayashi H, Hara K, Fukuoka A (2011) Hydrodeoxygenation of phenols as lignin models under acid-free conditions with carbon-supported platinum catalysts. Chem Comm 47(44):12209. https://doi.org/10.1039/C1CC14859A
22. Vasilevich AV, Baklanova ON, Lavrenov AV (2020) Hydrodeoxygenation of guaiacol with molybdenum-carbide-based carbon catalysts. Chem Select 5(15):4575–4579. https://doi.org/10.1002/slct.202000361
23. Jung KB, Lee J, Ha J-M, Lee H, Suh DJ, Jun C-J, Jae J (2018) Effective hydrodeoxygenation of lignin-derived phenols using bimetallic RuRe catalysts: effect of carbon supports. Catal Today 303:191–199. https://doi.org/10.1016/j.cattod.2017.07.027
24. Martínez-Klimov M, Mäki-Arvela P, Vajglova Z, Alda-Onggar M, Angervo I, Kumar N, Eränen K, Peurla M, Calimli MH, Muller J, Shchukarev A, Simakova IL, Murzin DY (2021) Hydrodeoxygenation of isoeugenol over carbon-supported Pt and Pt-Re catalysts for production of renewable jet fuel. Energy Fuels 35:17755–17768. https://doi.org/10.1021/acs.energyfuels.1c02656
25. Martinez-Klimov M, Mäki-Arvela P, Çiftçi A, Kumar N, Eränen K, Peurla M, Hensen EJM, Murzin DY (2022) Bifunctional Pt–Re catalysts in hydrodeoxygenation of isoeugenol as a model compound for renewable jet fuel production. ACS Eng Au 2(5):436–449. https://doi.org/10.1021/acsengineeringau.2c00015
26. Chen M-Y, Huang Y-B, Pang H, Liu X-X, Fu Y (2015) Hydrodeoxygenation of lignin-derived phenols into alkanes over carbon nanotube supported Ru catalysts in biphasic systems. Green Chem 17(3):1710–1717. https://doi.org/10.1039/C4GC01992J
27. Vargas-Villagrán H, Flores-Villeda MA, Puente-Lee I, Solís-Casados DA, Gómez-Cortés A, Díaz-Guerrero G, Klimova TE (2018) Supported nickel catalysts for anisole hydrodeoxygenation:

increase in the selectivity to cyclohexane. Catal Today 341:26–41. https://doi.org/10.1016/j.cattod.2018.07.057
28. Guan Q, Wan F, Han F, Liu Z, Li W (2016) Hydrodeoxygenation of methyl palmitate over MCM-41 supported nickel phosphide catalysts. Catal Today 259:467–473. https://doi.org/10.1016/j.cattod.2015.03.010
29. Fan X, Jiao Y (2020) Porous materials for catalysis: Toward sustainable synthesis and applications of zeolites. In: Sustainable nanoscale engineering, pp 115–137. Elsevier. https://doi.org/10.1016/B978-0-12-814681-1.00005-9
30. Choudary NV, Newalkar BL (2011) Use of zeolites in petroleum refining and petrochemical processes: recent advances. J Porous Mater 18:685–692. https://doi.org/10.1007/s10934-010-9427-8
31. Derouane EG, Vedrine JC, Pinto RR, Borges PM, Costa L, Lemos MA, Lemos F, Ribeiro F (2013) The acidity of zeolites: concepts, measurements and relation to catalysis: a review on experimental and theoretical methods for the study of zeolite acidity. Catal Rev 55(4):454–515. https://doi.org/10.1080/01614940.2013.822266
32. Whiting GT, Chung S-H, Stosic D, Chowdhury AD, van der Wal LI, Fu D, Zecevic Z, Travert A, Houben K, Baldus M, Weckhuysen BM (2019) Multiscale mechanistic insights of shaped catalyst body formulations and their impact on catalytic properties. ACS Catal 9:4792–4803. https://doi.org/10.1021/acscatal.9b00151
33. Murzin D (2020) Engineering catalysis. De Gruyter, Berlin, Boston. https://doi.org/10.1515/9783110614435
34. Vajglová Z, Kumar N, Peurla M, Hupa L, Semikin K, Sladkovskiy DA, Murzin DY (2019) Effect of the preparation of Pt-modified zeolite beta-bentonite extrudates on their catalytic behavior in n-hexane hydroisomerization. Ind Eng Chem Res 58(25):10875–10885. https://doi.org/10.1021/acs.iecr.9b01931
35. Cheng K, van der Wal LI, Yoshida H, Oenema J, Harmel J, Zhang Z, Sunley G, Zečević J, de Jong KP (2020) Impact of the spatial organization of bifunctional metal–zeolite catalysts on the hydroisomerization of light alkanes. Angewandte Chemie 132(9):3620–3628. https://doi.org/10.1002/ange.201915080
36. Vajglová Z, Simakova IL, Eränen K, Mäki-Arvela P, Kumar N, Peurla M, Tolvanen S, Efimov A, Hupa L, Peltonen J, Murzin DY (2022) The physicochemical and catalytic properties of clay extrudates in cyclization of citronellal. Appl Catal A 629:118426. https://doi.org/10.1016/j.apcata.2021.118426
37. Vajglová Z, Kumar N, Peurla M, Peltonen J, Heinmaa I, Murzin DY (2018) Synthesis and physicochemical characterization of beta zeolite-bentonite composite materials for shapedcatalysts. Catal Sci Technol 8:6150–6162. https://doi.org/10.1039/C8CY01951G
38. Vajglová Z, Kumar N, Mäki-Arvela P (2019) Synthesis and physico-chemical characterization of shaped catalysts of beta and Y zeolites for cyclization of citronellal. Ind Eng Chem Res 58:18084–18096. https://doi.org/10.1021/acs.iecr.9b02829
39. Emeis CA (1993) Determination of integrated molar extinction coefficients for infrared-adsorption bands of pyridine adsorbed on solid acid catalysts. J Catal 141:347–354. https://doi.org/10.1006/jcat.1993.1145
40. Murzin DY (2020) Engineering catalysis. In Engineering catalysis. de Gruyter. https://doi.org/10.1515/9783110614435
41. Leofanti G, Padovan M, Tozzola G, Venturelly B (1998) Surface area and pore texture of catalysts. Catal Today 41(1–3):207–219. https://doi.org/10.1016/S0920-5861(98)00050-9
42. Kubička D, Kumar N, Venäläinen T, Karhu H, Kubičková I, Österholm H, Murzin DY (2006) Metal-support interactions in zeolite-supported noble metals: influence of metal crystallites on the support acidity. J Phys Chem 110:4937–4946. https://doi.org/10.1021/jp055754k
43. Alda-Onggar M, Mäki-Arvela P, Eränen K, Aho A, Hemming J, Paturi P, Peurla M, Lindblad M, Simakova IL, Murzin DY (2018) Hydrodeoxygenation of isoeugenol over alumina-supported Ir, Pt, and Re catalysts. ACS Sustain Chem Eng **6**(12):16205–16218. https://doi.org/10.1021/acssuschemeng.8b03035
44. Bomont L, Alda-Onggar M, Fedorov V, Aho A, Peltonen J, Eränen K, Peurla M, Kumar N, Wärnå J, Russo V, Mäki-Arvela P, Grénman H, Lindblad M, Murzin DY (2018) Production of cycloalkanes in hydrodeoxygenation of isoeugenol over Pt- and Ir-modified bifunctional catalysts. Eur J Inorg Chem 24:2841–2854. https://doi.org/10.1002/ejic.201800391